IEEE Access
Multidisciplinary | Rapid Review | Open Access Journal

Received 24 September 2024, accepted 15 October 2024, date of publication 21 October 2024, date of current version 30 October 2024.

Digital Object Identifier 10.1109/ACCESS.2024.3484003

RESEARCH ARTICLE

Multi-Tb/s Transmission Based on DMT-Modulated VCSELs in Metro Networks Assisted by Volterra Equalization

ALBERTO GATTO[1], (Member, IEEE), ANTONINO FAVANO[1], PAOLA PAROLARI[1], (Senior Member, IEEE), CHRISTIAN NEUMEYR[2], MARCO FERRARI[3], (Member, IEEE), LUCA BARLETTA[1], (Member, IEEE), MAURIZIO MAGARINI[1], (Member, IEEE), AND PIERPAOLO BOFFI[1], (Senior Member, IEEE)

[1]Dipartimento di Elettronica, Informazione e Bioingegneria (DEIB), Politecnico di Milano, 20133 Milano, Italy
[2]Vertilas GmbH, Garching, 85748 Munich, Germany
[3]Italian National Research Council (CNR), 10129 Turin, Italy

Corresponding author: Alberto Gatto (alberto.gatto@polimi.it)

This work was supported in part by the European Union Horizon2020 PASSION project GA 780326, and in part by the Italian Ministry of University and Research PRIN2017 FIRST Project GA 2017HP5KH7_002.

ABSTRACT The effectiveness of Volterra equalization (VE) is analyzed to improve the performance of a metropolitan area network (MAN), characterized by directly-modulated (DM) vertical-cavity surface-emitting laser (VCSEL) sources combined with coherent detection, in order to target both high capacity and hundreds of km reaches. VE, which is a well-known nonlinear equalization technique, is used to cope not only with the distortion introduced by the real implementation of direct discrete multi-tone (DMT) modulation of the VCSEL, but also with the nonlinear impairments. A suitable experimentation, in case of 25-GHz spaced dense wavelength division multiplexed (DWDM) propagation, allows to validate a simulation tool, developed to provide a systematic analysis of the supported capacity per VCSEL, with and without VE. Simulations permit to analyze the effects of VE for different channel spacings (25, 50 and 100 GHz) and for different standard single-mode fiber (SSMF) lengths (up to 200 km), focusing on the evolution of the capacity per channel in case of different launch powers and optical signal-to-noise ratios. The dependence of the VE effectiveness is evaluated also in terms of spectral behavior. VE allows to achieve up to 13%-capacity increase, assuring 50 Gb/s rate per polarization per VCSEL, in case of DWDM transmission and after 200-km propagation, as targeted by the considered MAN applications.

INDEX TERMS Volterra equalizer, DMT modulation, MAN networks, direct modulation, VCSEL sources.

I. INTRODUCTION

Recently, many nonlinear equalization (NLE) techniques implemented through digital signal processing (DSP) have been proposed in literature [1], [2] to compensate for nonlinear distortions in optical communications systems. Among these, the Volterra equalizer (VE) [3] appears to be very interesting due to its capability to model complex dispersive nonlinear functions. Volterra equalizers operating either in the frequency [4] or in the time domain [5] have been successfully applied to different contexts, also considering the impact of their computational complexity and real-time implementation [6], [7].

In an optical communications system, VE is effective to partially face the nonlinear distortions, induced by the Kerr effect during propagation, but mainly the NLs arising along the modulation and detection chain (electrical amplifiers, digital-to-analog and analog-to-digital converters, RF drivers and modulators, photodiodes) [8]. These issues are relevant, above all in short and medium reach applications, where

The associate editor coordinating the review of this manuscript and approving it for publication was Rentao Gu.

propagation NLs, such as self-phase modulation (SPM), cross-phase modulation (XPM) and four-wave mixing (FWM), become less dominant although the channel high power and the dense spacing in case of wavelength-division multiplexing (WDM) can induce not negligible impairments. In [9] VE has been explored to compensate NLs caused by the employed transmitter (TX) and receiver (RX) components, comparing different single-carrier (SC) modulation formats with orthogonal frequency-division multiplexing (OFDM) format in a coherent system operating with a very high-bandwidth external IQ modulator.

For intra and inter data-center interconnections (DCIs), the effectiveness of VE has been demonstrated to support hundreds of Gb/s transmission in a few km of standard single-mode fiber (SSMF) [10], also in presence of direct detection (DD), where the square-law detection represents another nonlinear distortion source, owing to the signal-signal beat interference (SSBI). Moreover, VE at the TX side [11], based on pre-processing with pre-calculated filter's coefficients given by a look-up table, has been also utilized in such scenarios.

For DCIs and short-reach applications, the exploitation of low-cost and energy efficient laser sources, such as vertical-cavity surface-emitting lasers (VCSELs) directly modulated (DM) by multiple carrier formats such as discrete multi-tone (DMT) modulation, appears to be very promising. In the last years, strong progresses in the development of single-mode long-wavelength VCSELs working in the O- and C-band have been achieved, permitting to envisage their employment also in future medium-reach optical metropolitan area networks [12]. Despite the limited modulation bandwidth of the current VCSELs operating in the C-band, DMT permits to achieve high data rates, also allowing a dynamic and flexible adaptation to the specific traffic/channel conditions [13]. Volterra equalization has been employed in single-channel DMT-directly modulated sources [14] in case of DD over up to tens of kilometres of uncompensated SSMF, to compensate the nonlinear distortion induced by fiber chromatic dispersion (CD) and square-law detection, increasing the capacity of the DMT system. On the other hand, in case of medium-reach CD-compensated transmission, it would be worth to analyse VE capability to compensate the nonlinear response associated with DMT modulation of VCSEL sources. A DMT signal, in fact, is characterized by a large modulation dynamic range and is more sensitive to propagation NLs, owing to the high peak-to-average power ratio (PAPR); moreover, especially in case of high bias currents, owing to the internal heating effect [15], VCSELs show a highly nonlinear response.

DMT-modulated VCSELs could be considered an interesting option for medium-reach wavelength division multiplexed (WDM) links, such as metropolitan area networks (MANs) [12], where sustainable solutions in terms of cost, power consumption, and footprint are mandatory. An innovative TX module, covering the whole C-band and able to assure 2-Tb/s capacity per photonic integrated circuit (PIC), has been designed and implemented [16], [17], [18] by using DMT-modulated long-wavelength InP VCSEL sources [19], [20], [21], [22], achieving at least 50 Gb/s rate per state of polarization/wavelength. Dense WDM (DWDM) with 25-GHz spacing is enabled by single-sideband (SSB) filtering to provide multi-Tb/s throughput together with coherent detection (COD), in order to compensate for the CD and guarantee SSMF transmission reach of hundreds of kilometers [23].

Although the exploitation of VE has been already demonstrated in VCSEL-based systems exploiting DMT modulation [14], the effectiveness of VE in that uncompensated scenario has been analysed mainly to address the nonlinear distortions introduced by the direct modulation of the VCSEL and by the interaction between CD and square-law detection. Up to now, no extensive analysis of VE performance and features has been reported for transmissions in DWDM scenarios with DM signals on hundreds of kilometres propagation. In this paper, we report an experimental and simulative systematic analysis of the effectiveness of VE in a DMT-modulated VCSEL-based system in presence of dense WDM transmissions in a metro-haul scenario. The equalizer is employed not only to compensate for the distortions caused by the transmitter/receiver ends, but also to mitigate the impact of nonlinear impairments induced by the propagation over hundreds of fiber kilometers. The main outcomes presented in the paper are:

- the experimental evaluation of the effectiveness of VE in terms of achievable bitrate per VCSEL in a DMT-based multichannel metropolitan scenario exploiting direct modulation and coherent detection. The performance are measured in case of single-channel and multichannel conditions down to 25-GHz spacing;
- the development of a suitable simulative tool validated by the experimental results, able to correctly estimate the impact of TX/RX limitations, fiber NLs and VE application;
- the systematic analysis of the impact of VE on a DMT DM/COD VCSEL-based communication system in a DWDM scenario. The effectiveness of VE is analyzed for different channel spacings (25, 50 and 100 GHz) and for different SSMF lengths (up to 200 km), focusing on the evolution of the capacity per channel in case of different launch powers and optical signal-to-noise ratios (OSNRs). The VE effectiveness is evaluated also in terms of spectral behavior, analyzing the SNR profile of the DMT signal in different conditions;
- the evaluation of the optimal launch power per channel in the metro-haul scenario as a function of propagation length/conditions.

To the best of our knowledge, this is the first systematic analysis of VE behavior in DM/COD DMT signals in a DWDM metro communication system.

The paper is organized as follows. The description of VE is reported in Section II, while experimental results are shown in Section III. Moreover, the validation of the developed

simulative tool is provided. Thereafter, in Section IV the behavior of a VCSEL-based metro link is simulated in different conditions in terms of co-propagating channel number (from single channel to 7-channel condition) up to 200-km SSMF transmission. The performance of the envisaged system is reported in terms of capacity per channel supported with and without VE, while the effects of intra- and inter-channel NLs in both equalization conditions are analyzed. The performance is evaluated in terms of achievable capacity in function of both the propagation distance and OSNR/launch power. Finally, the impact of NLs and VE is analyzed in the spectral domain, in order to highlight the equalization behavior in different frequency regions.

II. VOLTERRA EQUALIZATION

A. GENERAL FORMULATION

Let us introduce the general formulation for a discrete-time VE. The resulting mth equalized sample at the output of a Kth order VE is defined as [3]

$$\begin{aligned} y(m) &= \sum_{k=1}^{K} \sum_{n_1=0}^{l_k-1} \sum_{n_2=0}^{n_1} \cdots \sum_{n_k=0}^{n_{k-1}} w_k(n_1, n_2, \ldots, n_k) \\ &\quad \cdot x(m-n_1)x(m-n_2)\ldots x(m-n_k) \\ &= \sum_{k=1}^{K} \sum_{n_1=0}^{l_k-1} \sum_{n_2=0}^{n_1} \cdots \sum_{n_k=0}^{n_{k-1}} w_k(n_1, n_2, \ldots, n_k) \\ &\quad \cdot x_{n_1} x_{n_2} \ldots x_{n_k}, \end{aligned} \tag{1}$$

where $x_n = x(m-n)$ is the sampled received signal at the input of the VE, while l_k and $w_k(n_1, n_2, \ldots, n_k)$ are, respectively, the memory length and the weights of the equalizer for the order $k = 1, \ldots, K$. In [5], the authors provide a computational complexity analysis as the order K increases and a reduced-complexity scheme for a second order VE. Since optical communication systems are typically affected by both second and third order nonlinearities [5], [6], [7], we extend the reduced-complexity scheme in [5] to the third order. For $K = 3$, the mth equalized sample is

$$\begin{aligned} y(m) &= \sum_{n_1=0}^{l_1-1} w_1(n_1)x_{n_1} + \sum_{n_1=0}^{l_2-1} \sum_{n_2=0}^{n_1} w_2(n_1, n_2)x_{n_1}x_{n_2} \\ &\quad + \sum_{n_1=0}^{l_3-1} \sum_{n_2=0}^{n_1} \sum_{n_3=0}^{n_2} w_3(n_1, n_2, n_3)x_{n_1}x_{n_2}x_{n_3}. \end{aligned} \tag{2}$$

We can express Eq. (2) in vector notation as

$$\begin{aligned} y(m) &= \sum_{p=1}^{l_1} [w_1 \circ x_{1,m}]_p + \sum_{p=1}^{l_2} \sum_{q=1}^{l_2} [w_2 \circ x_{2,m}]_{p,q} \\ &\quad + \sum_{p=1}^{l_3} \sum_{q=1}^{l_3} \sum_{r=1}^{l_3} [w_3 \circ x_{3,m}]_{p,q,r}, \end{aligned} \tag{3}$$

where the operator $\circ$ denotes the Hadamard product, $[\cdot]_p$ selects the pth element of a vector, $[\cdot]_{p,q}$ selects the element (p, q) of a matrix, and $[\cdot]_{p,q,r}$ selects the element (p, q, r) of a 3D matrix. We define the $l_1 \times 1$ vectors w_1 and $x_{1,m}$ as

$$w_1 = [w_1(0), \ldots, w_1(l_1-1)]^T, \tag{4}$$

$$x_{1,m} = [x_0, \ldots, x_{l_1-1}]^T. \tag{5}$$

The elements of the $l_2 \times l_2$ matrices w_2 and $x_{2,m}$ are, for $p + q - 2 < l_2$

$$[w_2]_{p,q} = w_2(p-1,\ p+q-2), \tag{6}$$

$$[x_{2,m}]_{p,q} = x_{p-1} \cdot x_{p+q-2}, \tag{7}$$

while they are set to 0 if $p + q - 2 \geq l_2$. In other words, both w_2 and $x_{2,m}$ are matrices with zero entries below their anti-diagonal. Finally, for $p + q + r - 3 < l_3$, the elements of the $l_3 \times l_3 \times l_3$ 3D matrices w_3 and $x_{3,m}$ are defined as

$$[w_3]_{p,q,r} = w_3(p-1,\ p+q-2,\ p+q+r-3), \tag{8}$$

$$[x_{3,m}]_{p,q,r} = x_{p-1} \cdot x_{p+q-2} \cdot x_{p+q+r-3}, \tag{9}$$

while the elements with indexes such that $p+q+r-3 \geq l_3$ are set to 0.

Since the VE implementation can become computationally complex even for relatively small values of l_k, a simplified model is required for practical implementations. Similarly to the approach used in [5], for the 2nd order VE, the model in (3) can be simplified by assigning independent and shorter memory lengths to the indexes p, q, and r. Therefore, this simplified scheme allows us to reduce the total number of taps for the Volterra weights and provides a flexible solution to adjust the trade-off between computational complexity and performance of the VE, making its implementation more practical. The reduced memory length for w_1 and $x_{1,m}$ is defined as $l_{1,p} \leq l_1$. For the rows and columns of w_2 and $x_{2,m}$ the reduced memory lengths are, respectively, $l_{2,p} \leq l_2$ and $l_{2,q} \leq l_{2,p}$. Finally, we have $l_{3,p} \leq l_3$, $l_{3,q} \leq l_{3,p}$, and $l_{3,r} \leq l_{3,q}$ for the rows, columns, and pages of w_3 and $x_{3,m}$. By plugging the reduced memory lengths into (3), the resulting mth equalized sample is

$$\begin{aligned} y(m) &= \sum_{p=1}^{l_{1,p}} [w_1 \circ x_{1,m}]_p + \sum_{p=1}^{l_{2,p}} \sum_{q=1}^{l_{2,q}} [w_2 \circ x_{2,m}]_{p,q} \\ &\quad + \sum_{p=1}^{l_{3,p}} \sum_{q=1}^{l_{3,q}} \sum_{r=1}^{l_{3,r}} [w_3 \circ x_{3,m}]_{p,q,r}. \end{aligned} \tag{10}$$

B. WEIGHTS ESTIMATION

Since the optimal VE weights w_k and their memory lengths l_k are not known, it is necessary to estimate them. Thanks to its computational simplicity and adaptation capabilities, the least-mean squares (LMS) algorithm [24] is one of the most viable solutions to accomplish this task [5]. Let $\{x(m)\}$ be a known and sufficiently long training sequence. The estimates of w_k are iteratively updated by employing an LMS algorithm. Let us denote by $\hat{w}_k(i)$ the ith estimate of the weight w_k. The iterative updates via LMS algorithm are

defined as follows

$$\hat{w}_1(i+1) = \hat{w}_1(i) + \mu_1 e_m x_{1,m}, \tag{11}$$
$$\hat{w}_2(i+1) = \hat{w}_2(i) + \mu_2 e_m x_{2,m}, \tag{12}$$
$$\hat{w}_3(i+1) = \hat{w}_3(i) + \mu_3 e_m x_{3,m}, \tag{13}$$

where $e_m = x(m) - y(m)$ is the instantaneous error and μ_k are the LMS step sizes. Finally, the estimated weights $\hat{w}_k$ can be plugged into (10) to implement the Volterra equalization.

III. EXPERIMENTAL RESULTS

A. EXPERIMENTAL SETUP

For the transmission performance evaluation, we employed the experimental setup shown in FIGURE 1(a). The channel under test (CUT) is obtained by a 15-GHz short-cavity (SC) InP VCSEL [25], [26] emitting in the C-band, directly modulated by a DMT signal generated by a MICRAM 100-GS/s digital-to-analog converter (DAC10002) with 35-GHz electrical bandwidth and 6 bits vertical resolution. The DMT signal is calculated by Matlab ® and is composed of 256 sub-carriers in 20-GHz range; a cyclic prefix (CP) of about 2.1% of the symbol length is added. The VCSEL emitting wavelength is 1534.5 nm, while its measured linewidth is about 5 MHz. The bias current is set at 9 mA, while the modulation depth is fixed at 450 mV in order to limit the frequency chirp insurgence and reduce the penalty due to single sideband (SSB) filtering [27]. A Finisar Waveshaper 4000s, which mimics the transfer function of a 25-GHz standard Wavelength Selective Switch (WSS) [28], further performs the single sideband filtering operation thanks to 8-GHz detuning with respect to the VCSEL carrier. The correct frequency detuning is achieved by operating on the VCSEL bias and temperature working conditions, as performed in the envisaged 2-Tb/s PIC modules [17], [18]. Moreover, it acts as a 25-GHz multiplexer, adding other two optical channels with ±25 GHz frequency difference with respect to the CUT. The adjacent channels are generated by modulating two 100-kHz tunable lasers by two Mach-Zehnder (MZ) intensity modulators with 25-GHz bandwidth and by tuning them at ±25 GHz from the CUT. The electrical DMT signals of the adjacent channels are generated by a second DAC (DAC10002) and, in order to decorrelate the patterns of the adjacent channels, a suitable 3-km long SSMF spool has been used (indicated as L_1 in FIGURE 1(a)). The adjacent channels undergo SSB filtering passing through the WS4000s multiplexer.

The generated single-polarization optical signal is then amplified by an Erbium-doped fiber amplifier (EDFA) and propagates in selected SSMF spools depending on the specific transmission distance with different launch powers. The employed spool lengths are shown in the inset of FIGURE 1(a), while the tested propagation distances are reported in TABLE 1. After SSMF propagation, the CUT is selected by a Finisar WS1000s programmable filter, which mimics the same transfer function of the multiplexer. Then,

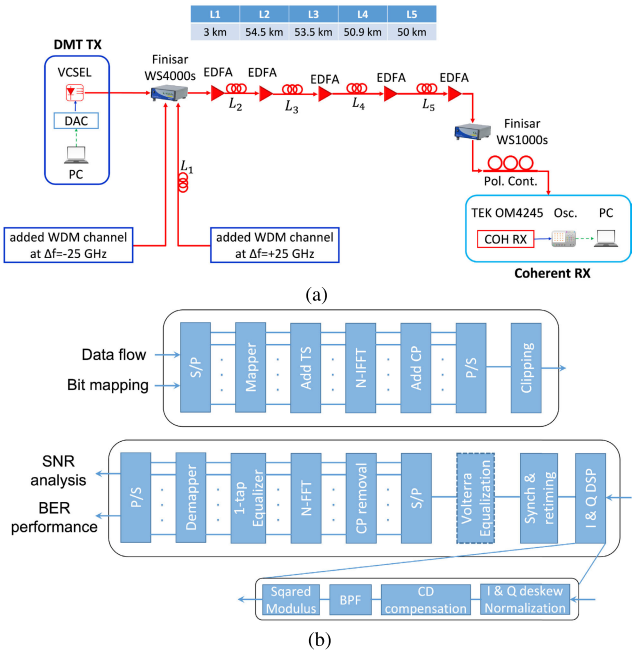

FIGURE 1. (a) Experimental setup. (b) TX and RX DSP architecture.

TABLE 1. Total propagation distances used during the experimental testing.

L_2	L_3	L_4	L_5	Total length [km]
√	×	×	×	54.5
√	√	×	×	108
√	√	√	×	158.9
√	√	√	√	208.9

to fully compensate the CD cumulated during propagation, the signal is detected by a Tektronix coherent receiver OM4245 with 45-GHz bandwidth. The local oscillator (LO) is a tunable 100-kHz laser with +14.5 dBm optical power. The in-phase/quadrature (I/Q) signals are acquired by a Tektronix real-time oscilloscope with 8-bits vertical resolution, 100-GS/s and 33-GHz electrical bandwidth, respectively. SSB DMT modulation is performed to enable higher spectral efficiency and 25-GHz granularity, while fully exploiting the SC-VCSEL envisaged bandwidth [21]. Optimal bit and power loading (BL/PL) using Chow's algorithm [29] is applied to adaptively assign the appropriate bit order at each subcarrier during the mapping procedure. This strategy enables to finely tailor the spectrum with a granularity of tens of MHz, allowing also MAN functionalities such as multi-flow generation, slice-ability, adaptability to traffic and reach [13], [30], [31]. In case of 256 subcarriers occupying 20-GHz bandwidth, the resulting granularity is about 78 MHz.

FIGURE 1(b) reports the DSP fundamental blocks. At the TX side, the DSP performs serial-to-parallel conversion (S/P), bit mapping of the digital/electrical subcarriers, adding of training symbols (TS), inverse fast Fourier transform (IFFT), adding of CP and parallel-to-serial operation (P/S); finally, the resulting signal is clipped and can be

electrically-generated by a suitable DAC. The same steps in reverse order are performed by the RX, for retrieving the transmitted data from the analog-to-digital converter (ADC). Thanks to the exploitation of direct modulation at the TX side, it is possible to implement a simplified coherent detection scheme based on the application of a digital square modulus to the I/Q components, thus not requiring a full carrier recovery. Firstly, the digitized I/Q components are de-skewed, orthogonalized, and normalized, in order to optimally combine them, obtaining the proper complex representation of the optical signal. Afterwards, CD is totally compensated, by employing a suitable digital filter operating in the frequency domain, tailored to each propagation distance; a digital band-pass filter (BPF) is applied and the squared modulus function is performed. The filter is specifically designed to improve the performance of the optical SSB filtering, while rejecting out-of-band noise components. Therefore, its response is expected to feature sharp edges and a rather limited bandwidth. The envisaged simplified CO-Rx relaxes the requirements in terms of phase noise of signal source and LO, needing just few-MHz laser linewidths, typical of currently-deployed SC-VCSELs [32]; on the other hand, the SNR gain of COD with respect to DD is lost. Then, a synchronization and retiming (down-sampling) procedure is applied to obtain a suitable baseband DMT signal; (where appropriate) Volterra equalization is applied to the time-domain signal. The assessment of the optimal VE weights is performed during the first step of the bit/power loading algorithm, in which the SNR of the different sub-carriers is estimated by the transmission of a suitable signal uniformly-loaded by QPSK. The optimization of the weights is performed for each system condition and propagation distance, leading to different estimates for single-channel and multichannel transmissions. After the first estimation of the VE weights, the coefficients are adaptively updated using a LMS algorithm. Afterwards, S/P is applied, CP removed, and FFT performed. Finally, after the implementation of standard one-tap equalization to correctly re-phase the subcarriers constellations, the multicarrier signal is demapped and serially converted. The performance of the system is evaluated in terms of capacity achievable for a target BER of $4.62 \cdot 10^{-3}$ (consistent with the use of a 7% overhead HD-FEC [33]), whereas the analysis of the SNR per sub-carrier is performed to highlight the impact of NL propagation on DMT signals in the spectral domain.

B. EXPERIMENTAL RESULTS AND MODELING

The capacities achieved after 100-km SSMF propagation in function of the total optical launch power are reported in FIGURE 2(a). In particular, the performance of the system has been experimentally measured in case of single-channel and multichannel transmissions (full marks). The evolution of the capacity in function of the launch power follows the standard parabolic shape determined by the presence of NL impairments. In particular, the optimal launch power in case

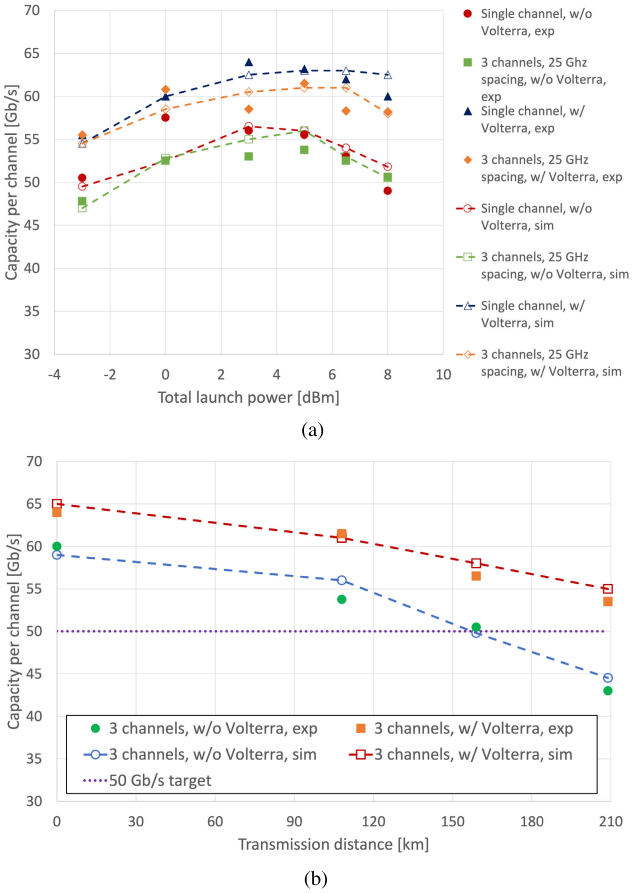

FIGURE 2. (a) Experimental results for single channel and multichannel transmissions on 100-km SSMF (full marks). (b) Supported measured capacities per channel versus SSMF length with and without nonlinear Volterra equalization in case of 3 co-propagating 25-GHz-spaced channels transmission (full marks). Numerical model in the same conditions (empty marks, dashed lines).

of single-channel transmission (red full circles) is close to 3 dBm, whereas in case of multichannel propagation (green full squares) it is 5 dBm, corresponding to a power per channel around 0 dBm. The optimal condition is obtained for the same optical powers also when exploiting the VE (blue triangles and orange diamonds), evidencing that even with NL equalization the channel performance is more affected by the XPM presence. Of course, an increase in the capacity is gained by applying the NL equalization, with a percentage improvement close to 15%. The capacities achieved in the multichannel condition are around 62 Gb/s and 54 Gb/s with and without VE, respectively.

The performance of the multichannel transmission has been analyzed for different SSMF propagation lengths, up to 210 km. In particular, in FIGURE 2(b) the capacities achievable at the optimal launch power for each propagation distance with and without VE are reported. As expected, the capacity reduces with increasing transmission distance due to a reduction of the achievable OSNR at different SSMF lengths. Moreover, as visible in particular in absence of VE for SSMF lengths beyond 100 km, strong non-

linear impairments, accumulated during SSMF propagation, further reduce the achievable capacity. Without VE, the 50-Gb/s target capacity can be guaranteed only up to 150 km, with a rapid decrease of the performance for longer distances, as pointed out by a maximum capacity of 43 Gb/s after 200-km SSMF transmission. On the other hand, the application of VE permits to compensate both the intrinsic NL impairments of the transmission system, as evident from back to back performance, and the NL effects arising from fiber propagation. The mitigation of fiber NL impairments appears for transmissions beyond 100 km, as highlighted by the different slopes of the capacity evolution with and without VE. The application of Volterra equalization permits to obtain about 54 Gb/s after 200-km SSMF propagation, guaranteeing to achieve the 50-Gb/s target capacity even for longer distances.

The reported measurements have been used to validate a simulative tool [21], able to model all the different devices/components exploited during the experimental tests. It is based on Matlab^{TM} and it includes all the transmission, propagation, filtering and receiver functionalities. The 45-GHz OM4245 Tektronix coherent detector has been modeled in terms of electrical noise power density and responsivity, while the simulated LO power has been set to 14.5 dBm as in the measurements. The DM VCSEL is modeled considering both the intrinsic modulation properties and the extrinsic device parasitic components, following the approach reported in [34], leading to the equivalent electrical modulation frequency response close to 15 GHz. The impact of optical filtering at multiplexing and demultiplexing stages is evaluated using the experimentally measured 25-GHz WSS transfer function [28] generated by the Finisar Waveshaper WS4000 programmable filter. The optical propagation is performed using the split-step Fourier method, in order to solve the nonlinear Schrödinger equation for both the signal polarizations. It accounts for linear and nonlinear propagation effects, as chromatic dispersion and Kerr-related NLs. The measured OSNRs have been used for the different launch power conditions both for the single-channel and multichannel transmissions.

The precise modeling of the system considered in the experimental set-up allowed to perform accurate simulations. In FIGURE 3, examples of optical and electrical spectra are shown for the 25-GHz spaced 3-channel system configuration. In particular, FIGURE 3(a) represents the optical spectra experimentally-measured after 100-km SSMF propagation before and after the demultiplexing filter: the presence of the frequency chirp is evident for the central channel, generated directly-modulating the VCSEL source with the DMT signal; the two adjacent channels, on the other hand, show chirp-free spectra, thanks to the exploitation of external modulation. After the demultiplexer, just the residual presence of the CW carrier of the left channel can be noticed. Thanks to SSB filtering, the channels can be transmitted with 25-GHz spacing with a negligible spectral overlapping. Likewise, FIGURE 3(b) shows the optical spectra obtained by the

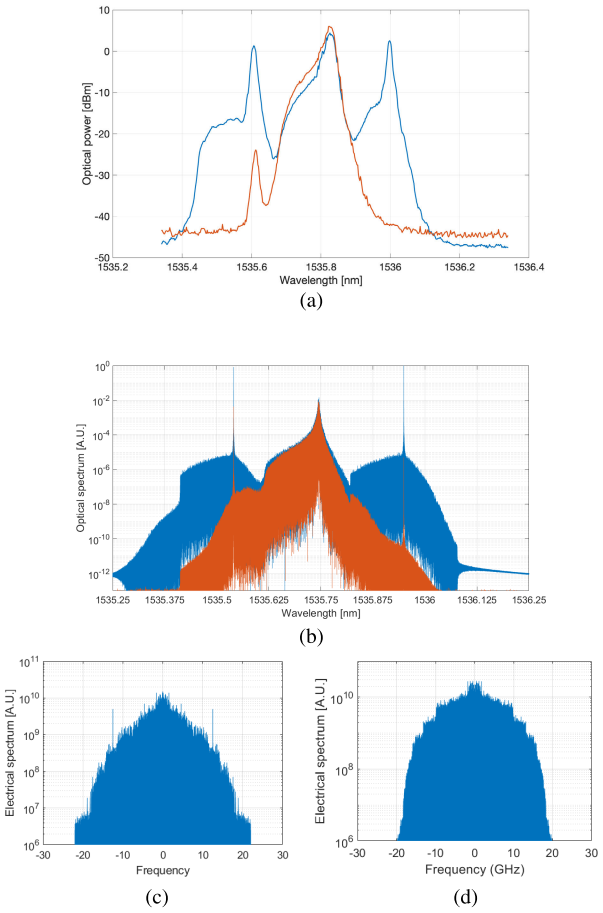

FIGURE 3. (a) Optical spectra of 25-GHz-spaced 3-channel transmission measured after 100-km SSMF before (blue curve) and after (red curve) the demultiplexer filter. (b) Optical spectra of 25-GHz-spaced 3-channel transmission simulated after 100-km SSMF before (blue curve) and after (red curve) the demultiplexing filter. (c) Example of electrical spectrum experimentally measured at the receiver. (d) Example of electrical spectrum obtained by simulations at the receiver.

simulation tool in the same conditions. Thanks to the higher frequency resolution achievable in the simulative analysis, the difference between VCSEL- and MZ-generated channels is more evident: the presence of the frequency chirp in the central channel appears as a widening of the optical spectrum, in particular in the frequency region close to the optical carrier. For the externally-modulated channels, on the other hand, the spectra in the optical domain are a replica of the electrical ones. Examples of electrical spectra obtained after the signal detection and DMT processing are reported in FIGURE 3(c)-(d) for DMT signals after bit loading. As expected, the electrical spectra show a step-like shape, owing to the bit and power loading procedures. The capacities obtained experimentally and with simulations are shown in FIGURE 2(a) and FIGURE 2(b) as dashed curves and empty marks, respectively. The experimental and simulative results are in quite good agreement both for single-channel and multichannel transmissions; the simulator well approximates the evolution of the channel capacity both in function of the

TABLE 2. Simulation parameters.

Parameter	Value
VCSEL bandwidth	15 GHz
VCSEL α parameter	3.7
VCSEL adiabatic factor κ	$1.53 \cdot 10^{13}$ Hz / W
DMT subcarrier number	256
RX bandwidth	45 GHz
WSS bandwidth	25 GHz
Number of channels	1, 3, 7
3-channels configuration spacing	25, 50, 75, 100 GHz
SSMF path length	0, 50, 100, 150, 200 km

launch power (FIGURE 2(a)) and of the propagation distance (FIGURE 2(b)), confirming that the developed tool is able to correctly estimate the performance in presence of SPM and XPM after NL propagation in hundreds of kilometer links. Moreover, the capacity is correctly estimated also in case of VE, permitting to exploit the developed tool to fully envisage the performance of a metro system at different link lengths.

IV. SIMULATION ANALYSIS

Extensive simulations have been performed to estimate the performance of the photonic system for the targeted metro distance (up to 200 km) considering several DM VCSELs co-propagating in the same fiber link. In particular, different channel configurations have been analyzed, in order to underline the impact of NL impairments such as SPM and XPM depending on the number and the spacing of the co-propagating channels. The performance of the photonic system has been measured in terms of supported capacity with and without VE. Table 2 reports the main parameters of the modelling and simulative assessment.

As previously described, a 45-GHz OM4245 Tektronix coherent detector has been emulated, with a 10-dBm LO with 100-kHz linewidth. The selected LO parameters are typical of commercial coherent detection systems. All the DM VCSELs are modeled considering both the intrinsic/extrinsic modulation properties [34] and the chirp behavior, leading to the VCSEL parameters reported in Table 2. Experimentally-measured 25-GHz WSS transfer functions [28] are exploited as multiplexing and demultiplexing stages. The considered propagation medium is a SSMF with 0.25 dB/km attenuation and 16 ps/nm km dispersion at 1545 nm. The OSNR at the receiver is varied according to the measurements for the 100-km propagation scenario; for the other SSMF path lengths, it is obtained assuming the presence of EDFAs with the same noise figure of the experimented ones (i.e., 6 dB). The SSB transmission is performed by properly detuning the WSS transfer functions with respect to the carrier of the DMT signal. Similar DSP blocks to those described in Section III-A are applied, performing suboptimal adaptive BL algorithm [29] and considering again the target BER of $4.62 \cdot 10^{-3}$ for single-polarization transmission [33]. The worst-case scenario of perfect polarization alignment of all the co-propagating channels is being thus analyzed.

Finally, FIGURE 4 reports the flowchart of the algorithm used to estimate the system performance in terms of

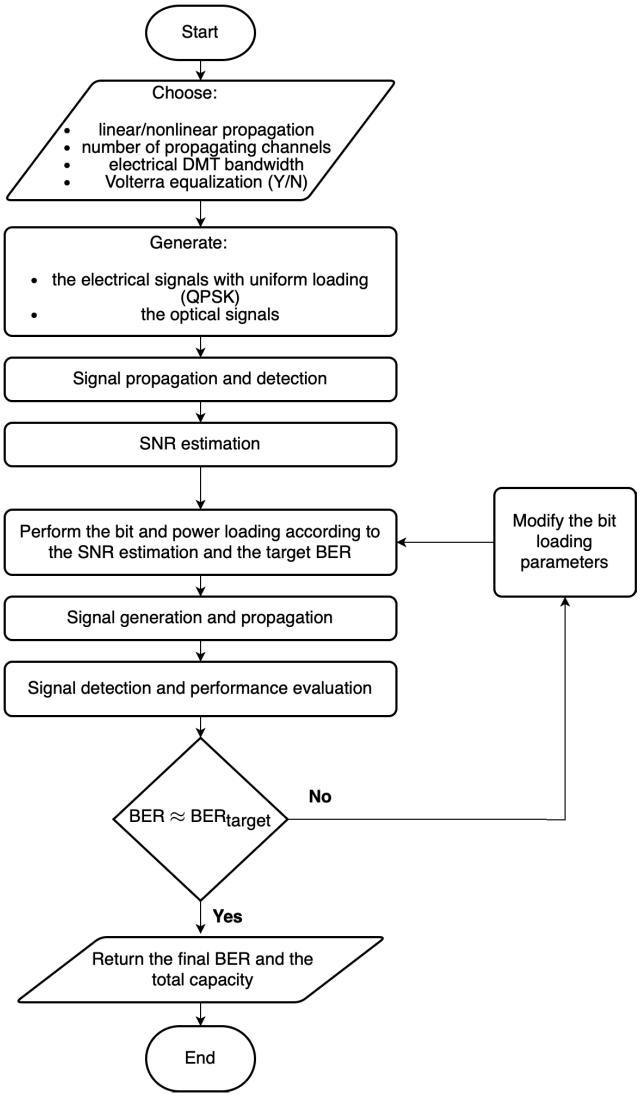

FIGURE 4. Flowchart of the algorithm used to calculate the performance of the VCSEL-based DMT system in terms of achievable capacity.

achievable capacity. Specifically, it starts by selecting the propagation behavior, the number of co-existing channels, the specifications of the electrical DMT signal and the presence or absence of the Volterra equalizer. Then, the estimation of the electrical SNR achievable per subcarrier is performed, using a uniformly-loaded DMT signal. After this first phase, the algorithm starts an iterative process to find the correct value of capacity that permits to obtain the specific target BER previously reported. In particular, the estimated SNR and the target BER are used to perform the bit and power loading procedures; after signal propagation and detection, the obtained BER value is compared to the target one. To end the iterative process, a maximum difference of $2 \cdot 10^{-4}$ between the current and target BER moduli is required. In case the difference is greater, the bit loading parameters are updated accordingly, while when the convergence condition is fulfilled, the algorithm stops and provides the calculated BER and total capacity transported by the channel under test.

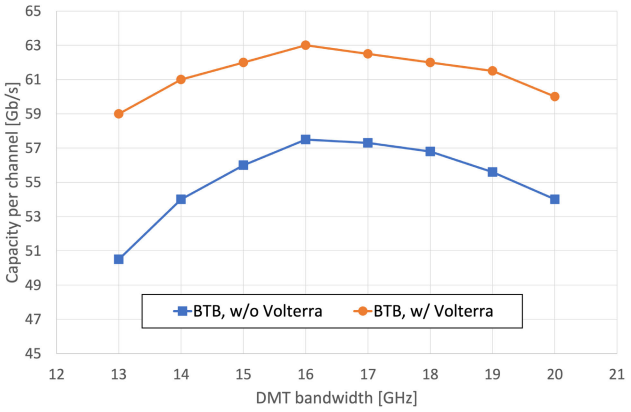

FIGURE 5. Supported capacities in function of DMT electrical bandwidth with (orange circles) and without (blue squares) Volterra equalization for multichannel transmission.

A. DMT MODULATION BANDWIDTH

Firstly, the optimal modulation bandwidth in case of VCSEL-based multichannel transmission has been found. Differently from external modulation, DM VCSELs are affected by a strong frequency chirp, which widens the channel optical spectrum. Since the envisaged photonic system is based on the multiplexing of DM VCSELs with a very tight spacing of 25 GHz, the chirp could be a limit in terms of frequency-dependent losses, generated by narrow optical filtering, and crosstalk among adjacent channels. As is well known, frequency chirp arising from direct modulation of VCSEL is composed of two distinct components, one proportional to the emitted optical power (adiabatic chirp) and another related to its derivative (transient chirp) [35]; therefore, the electrical spectrum of the DMT modulating signal directly affects the frequency chirp of the VCSEL source and, definitely, the width of the resultant optical spectrum after direct modulation. Hence, the performance of the metro photonic system was analyzed depending on the DMT modulation bandwidth, in order to optimize it to the specific requirements. In particular, the analysis has been carried out in case of multichannel propagation in back-to-back conditions, when the presence of different co-propagating channels with 25-GHz spacing could originate also an in-band crosstalk, affecting the transmission performance.

The supported capacities for different DMT electrical bandwidths with and without VE are reported in FIGURE 5. As expected, the capacity supported in presence of VE always outperforms the standard performance. Moreover, a stronger gain is obtained for narrow DMT modulation bandwidth, indicating that the equalizer is mainly working in the low/mid-frequency region of the electrical spectrum. Increasing the modulation bandwidth, a reduction can be noticed, due to the insurgence of the simultaneous partial filtering of the edge subcarriers and of crosstalk-induced capacity penalties, due to the presence of frequency chirp that widens the optical spectrum of the propagating channel [27]. In presence of crosstalk, the sub-carriers at the high-frequency edge experience a stronger noise level due to channel interference and, hence, the overall signal SNR decreases. In these conditions, the VE shows a reduction of its effectiveness, owing to the lower signal SNR. The adjacent-channels crosstalk, in fact, could be modeled as an additional noise contribution in the high-frequency region, whose occupancy is proportional to the DMT modulation bandwidth. Since noise is detrimental to VE, better performance can be obtained with a narrow DMT bandwidth. FIGURE 5 demonstrates that for both equalization conditions the maximum capacity is obtained for around 16-GHz DMT modulation bandwidth, which represents a trade-off between the capacity increase due to the wider bandwidth and the decrease owing to the adjacent channels chirp-induced crosstalk. This optimal value is determined also by the VCSEL electro-optical bandwidth, which is 15 GHz, as reported in Table 2; in this case, the VE allows a capacity improvement around 9%. Thus, a modulation bandwidth of 16 GHz has been exploited in all the simulations in the following sections.

B. VOLTERRA EQUALIZER CONFIGURATION

In Section II, we introduced the general formulation of a discrete-time third-order VE. Firstly, an estimation of the VE effectiveness has been performed, in order to optimize the number and convergence parameters of the Volterra weights by using the procedure described in Section II-B. To find a suitable VE configuration to be used in the following simulative analysis, we tested several sets of VE parameters by empirically adjusting the initialization of the weights $\hat{w}_k(0)$, the LMS step sizes μ_k, and the memory lengths l_k. This analysis has been performed at a propagation distance of 200 km with the presence of seven 25-GHz spaced channels; its results indicated that the VE performance negligibly improves when the memory length l_1 is above 4, the second-order memory length l_2 above (4, 2) and the third-order memory length l_3 above (4, 3, 2). In order to limit the computational complexity of the VE we thus fixed the above mentioned tap numbers.

Finally, we analyzed the convergence of the weights estimates. Since we assumed the channel to be fairly stable over time, we performed the LMS weights estimation just once during the initial training phase of the bit/power loading procedure, when the SNR of each subcarrier is estimated. We expect the weights re-estimations to be required just occasionally over time and therefore to have a negligible impact on the overall computational complexity of the system. As an example, in FIGURE 6 the evolution of second-order weights estimated via the LMS algorithm is shown as a function of iterative updates. Moreover, in red, the corresponding supported capacities, in Gb/s, obtained by increasing the length of LMS training sequences are reported for 4 different update numbers. The figure also shows how, after about $6 \cdot 10^5$ iterative updates, the second-order weights have reached a good convergence; further increments in the update number do not lead to any deviation of the supported capacity, as expected for weights at the

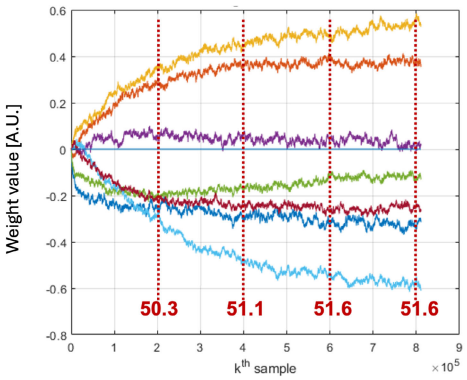

FIGURE 6. Iterative updates for the estimates of the 2nd order Volterra weights (represented by the different colors) with $l_{2,p} = 4$ and $l_{2,q} = 2$. In red, the supported capacities [Gb/s] achieved using the Volterra weights obtained after $[2, 4, 6, 8] \cdot 10^5$ iterative updates in the LMS estimation.

steady-state value. However, it is important to notice that even after $2 \cdot 10^5$ iterative updates a good improvement in terms of capacity can be achieved with respect to the reference one, suggesting that the VE quickly reaches a stable working condition and that the following iterative updates are needed just as a final refinement to maximize the performance of the channels. Actually, the other-order weights show comparable convergence time.

C. TRANSMISSION PERFORMANCE

FIGURE 7 shows the performance of the analyzed metro system in case of 200-km SSMF propagation in terms of capacities as a function of the optical launch power per channel for different configurations of co-propagating channels with (FIGURE 7(b)) and without (FIGURE 7(a)) NL VE. In particular, the single-channel configuration permits to evaluate the impact of SPM; by comparison, the 3-channel condition is used to highlight the impact of XPM depending on the channel spacing, which ranges from 25 GHz to 100 GHz; finally, the 7-channel configuration allows to assess the performance of the system when all C-band channels are switched on, being negligible the effect of a higher number of channels. As a reference, also the single-channel and 3-channel configurations in case of linear propagation are reported: the former represents the BTB performance of the single DM VCSEL, whereas the latter permits to evaluate the crosstalk impact of 25-GHz spaced WDM channels on the capacity.

As expected, due to the OSNR increase, in linear regime the capacity increases with the launch power; in case of multi-channel propagation (green dotted triangles) the capacity is reduced of a few Gb/s with respect to the single-channel condition (blue dotted circles) owing to the crosstalk of 25-GHz adjacent channels. Thanks to the choice of the DMT modulation bandwidth performed in Section IV-A, this impact is properly limited. In NL regime, the capacity shows the typical parabolic trend, with an initial increase (thanks to a better received OSNR) and a subsequent

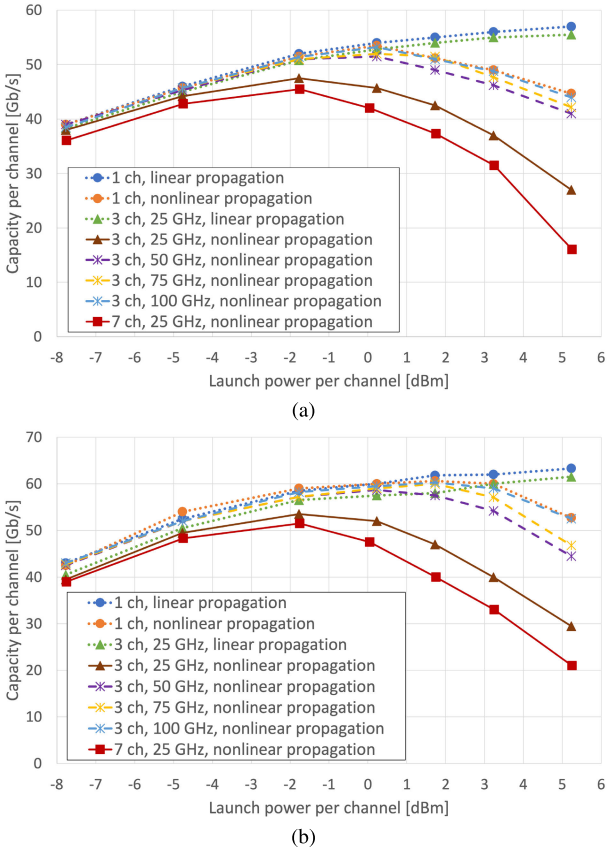

FIGURE 7. Performance in terms of capacity achieved after 200-km SSMF propagation without (a) and with (b) nonlinear VE.

reduction (owing to the impact of SPM and XPM). The 3-channels configuration was analyzed for different channel spacings to evidence the different NL behavior. In particular, the 100-GHz spacing curve matches the single-channel one, i.e., channels spaced 100 GHz do not add measurable XPM penalties to SPM ones. For this reason our further analyses are performed at 25-GHz, 50-GHz and 75-GHz channel spacings. In addition, this confirms that the NL penalty contribution of a number of 25-GHz spaced channels higher than 7 is negligible. On the other hand, reducing the channel spacing increases the XPM impact, starting from a very low penalty in case of 75-GHz spacing to a high impact for 25-GHz spaced channels. Moreover, whereas the curves down to 50-GHz spacing almost match the single-channel one up to the optimal launch power, in case of 25-GHz spacing there is a clear reduction of the supported capacity even for lower optical launch powers. The optimum launch power per channel is in fact around 0 dBm for single channel, 75-GHz and 50-GHz spacings, whereas for 25-GHz spacing configurations (3-channels and 7-channels) it is close to -1.5 dBm.

FIGURE 7(b) analyzes the use of VE; as expected, the performance of the transmission system improves, permitting to support higher capacities, up to 63 Gb/s in BTB. Moreover, the VE is effective also in the reduction of SPM penalties,

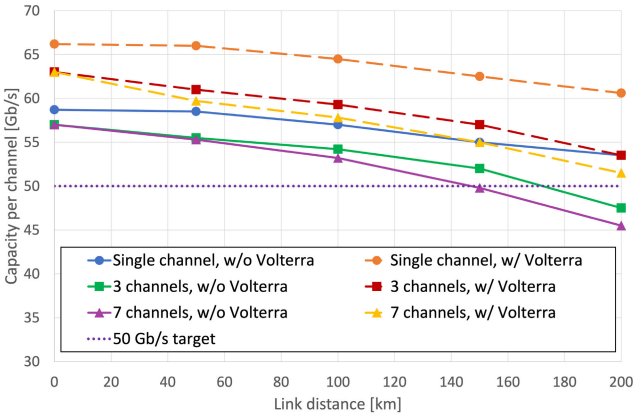

FIGURE 8. Supported capacities versus SSMF length with (dashed curves) and without (continuous curves) nonlinear Volterra equalization for single-channel (circles), 3-channels (squares) and 7-channels (triangles) transmissions. Multichannel performance are evaluated in case of 25-GHz spaced channels.

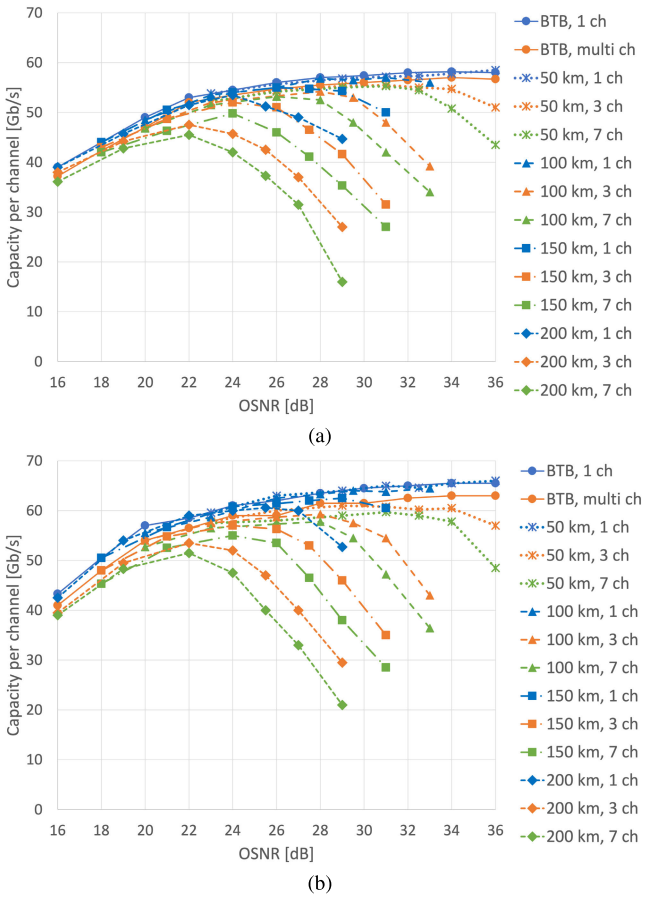

FIGURE 9. System performance in terms of capacity achieved versus received OSNR for different propagation distances without (a) and with (b) nonlinear Volterra equalization in case of single channel (blue), 3-channels (orange) and 7-channels (green) transmission. Multichannel performance are evaluated in case of 25-GHz spaced channels.

as visible from the single-channel NL propagation curve (dotted orange curve). In this case, the supported capacity increases up to 60 Gb/s, for +1.5 dBm launch power, whereas without the VE an optimal launch power of 0 dBm and a maximum capacity of 53 Gb/s are obtained. As without the VE, the 100-GHz channel spacing performance matches the single-channel one. On the other hand, in case of 25-GHz channel spacing (the highest XPM impact configuration), the reduction of the capacity with respect to the linear propagation regime for the optimal launch power is about 6.5%, as for the case without the VE. Volterra equalization confirms to be ineffective in mitigating inter-channel NLs. However, VE exploitation, thanks to transmission system NLs and SPM mitigation, allows to achieve a capacity of 51.5 Gb/s even in case of 7 channels with 25-GHz spacing up to 200 km of SSMF propagation.

Focusing on the photonic system based on 25-GHz spaced DM VCSELs, FIGURE 8 shows the maximum capacity that can be supported at different propagation distances with (dashed curves) and without (continuous curves) the VE; the 50 Gb/s target capacity to achieve multi-Tb/s transmission [12] is also reported (dotted purple curve). Volterra equalization permits to support more than 50 Gb/s even in case of multichannel propagation on up to 200 km, whereas in case of 7-channel propagation without VE this target capacity cannot be supported even after 150 km SSMF.

By comparing single-channel configurations with and without VE, it can be noticed that they both undergo a reduction of about 5 Gb/s after 200-km SSMF propagation; however, the capacity percentage reduction from BTB to 200 km is 7.6% and 9.3% with or without the VE, respectively. Therefore, the VE permits to recover not only all the initial signal distortions, starting with a higher capacity, but also part of the NL SPM penalty. Multichannel propagation reduces the achievable capacity: in case of 25-GHz spaced channels, even with VE the reduction is about 11% with respect to the single-channel condition, due to inter-channel NLs. After 200 km SSMF propagation and channel full loading, the overall capacity decrease with respect to single-channel BTB condition is about 22%.

D. CAPACITY VS OSNR

The performance of the proposed system architecture can be analyzed also in terms of total transported capacity versus the received OSNR levels. The OSNR measurement follows the approach proposed in [36] to evaluate the actual DMT-signal OSNR. In particular, FIGURE 9 shows the transmission performance for different propagation lengths (from BTB up to 200 km) and different channel conditions (single channel, 3 channels and 7 channels, both with 25-GHz spaced channels) to show the different impacts of intra- and inter-channel NLs on the system performance. In both equalization conditions, the impact of fiber NLs reveals as a capacity decrease after a threshold OSNR, corresponding to the optimal launch power. Considering single-channel curves, short-distance performances are not affected by significant SPM effect in the considered OSNR range, following the BTB behavior. By increasing the transmission distance, a decrease of the optimal OSNR

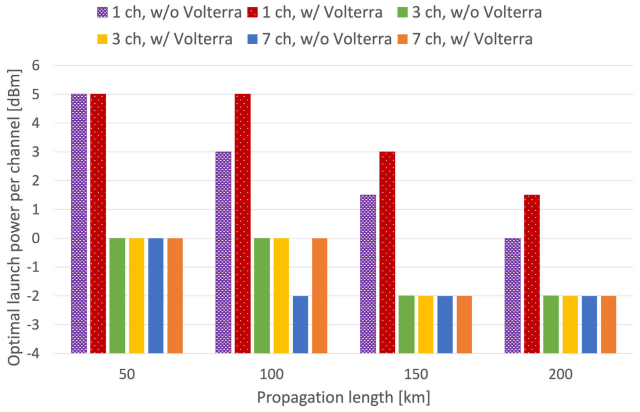

FIGURE 10. Optimal launch power for 50 km, 100 km, 150 km, 200 km SSMF transmission for propagation of: 1 channel without VE (purple) and with VE (red); 3 channels without VE (green) and with VE (yellow); 7 channels without VE (blue) and with VE (orange).

value can be noticed, reaching in case of 200-km SSMF propagation an optimum OSNR of 26 dB and 24 dB with and without VE, respectively. However, for all the considered propagation distances, the single-channel behavior perfectly follows the BTB curve up to the optimal OSNR value, deviating from it for higher OSNR values only. Therefore, the equalizer mitigates the effects of SPM on the channel performance, permitting to exploit a higher launch power.

By comparing single and multi-channel curves it is confirmed that VE is not effective in XPM mitigation. Moreover, since the performance of the equalizer depends on the initial SNR of the different sub-carriers composing the DMT signal, in case of 25-GHz channel spacing the CUT performance is also affected by the in-band crosstalk induced by the chirp, which actually lowers the overall signal SNR. A reduction of few Gb/s is experienced, with a higher impact on VE efficiency, as shown by the continuous orange curves in FIGURE 9. These multichannel BTB curves, anyway, represent the achievable capacities in a linear-propagation condition, thus they could be used as a reference for multi-channel behavior. The presence of XPM causes a shift of the optimal working point towards lower OSNRs, i.e., a reduction of the optimal launch power is expected increasing the propagating distance. After 200-km SSMF propagation, a loss of capacity with respect to BTB multi-channel situation (i.e., in linear regime) of about 8.9% and 12.5% are obtained with and without VE. These losses correspond to a capacity reduction of 5 Gb/s and 6.5 Gb/s, respectively.

Finally, FIGURE 10 shows the optimal launch power per channel for the different system configurations. As expected, the optimal launch power decreases with the transmission length and with the number of active 25-GHz spaced channels. Generally, in case of single-channel propagation the exploitation of VE permits to compensate the intra-channel NLs, allowing to use higher launch powers and, thus, leading to an increase of the OSNR at the receiver

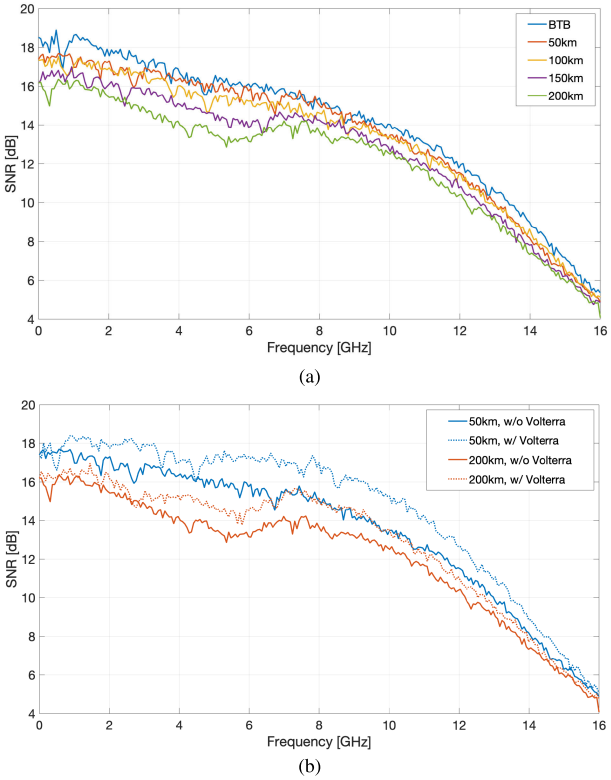

FIGURE 11. (a) SNR profiles obtained in BTB condition and after 50-km, 100-km, 150-km and 200-km SSMF non-linear propagation without Volterra equalization in the optimal working point in case of 7 25-GHz-spaced channels. The corresponding OSNR values are 36 dB, 31 dB, 26 dB, 24 dB and 22 dB, respectively. (b) SNR per sub-carrier at optimal launch power in case of 50-km (blue-light blue curves) and 200-km (red-orange curves) SSMF propagation with and without VE. The OSNR is 31 dB and 22 dB for the two different propagation lengths, respectively.

and, hence, to obtain superior total transported capacities. On the other hand, in case of multi-channel systems, it is possible to increase the launch power just for the 100-km reach, increasing the received OSNR and the performance, while for 150 km and 200 km the channel launch power is not affected by the employment of VE, not obtaining an OSNR advantage in case of multi-channel propagation.

E. SNR ANALYSIS

The impact of fiber non-linear propagation on directly-modulated DMT signals deserves to be analyzed also in the frequency domain. Thanks to the first step of the bit-loading technique, during which all the sub-carriers are loaded by a uniform QPSK modulation, it is possible to obtain a detailed description of the frequency-dependent impact of NLs by observing the SNR profile after different propagation distances in the two equalization conditions.

FIGURE 11(a) shows examples of the SNR per sub-carrier achieved after different SSMF lengths at the respective optimal launch power without activating the VE in case of 7-channel propagation. Since the SNRs are evaluated at the optimal working point for each propagation distance, the

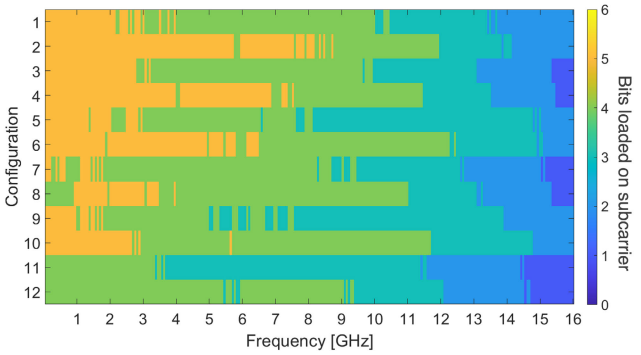

FIGURE 12. Examples of bit loading achievable with and without VE for single and 7-channels transmissions, in case of different propagation distances (BTB, 100 km and 200 km). The configurations are reported in TABLE 3.

TABLE 3. System configurations used for the bit loading analysis shown in FIGURE 12.

Configuration	Channels	SSMF length [km]	VE	$\sum_i b_i$
1	1	0	no	933
2	1	0	yes	1052
3	7	0	no	910
4	7	0	yes	1009
5	1	100	no	909
6	1	100	yes	1040
7	7	100	no	852
8	7	100	yes	923
9	1	200	no	852
10	1	200	yes	976
11	7	200	no	724
12	7	200	yes	823

curves correspond to different OSNRs, ranging from 36 dB for the BTB condition to 22 dB in case of 200-km propagation. The reduction of the OSNR leads to a general decrease of the SNR curve, easily visible by the lowering of the high-frequency region (from 8 GHz to 16 GHz). Sub-carriers at very high frequency, as the ones close to 15-16 GHz, are not so affected by the OSNR variation, since the initial SNR is too low to be correctly estimated. On the other hand, the effect of fiber NLs appears as an additional decrease in the low-frequency range, and as a wide frequency dip in the mid-frequency region, with the dip position depending on the cumulated NL phase modulation [37]. In particular, the SNR maintains the standard low-pass profile up to 100-km transmission, whereas a dip at 6 GHz and 5 GHz appears after 150 km and 200 km, respectively. The width and the depth of the frequency dip increase as the propagation distance. FIGURE 11(b) shows the impact of VE on the SNR curves. In particular, the SNR profiles corresponding to 50-km (blue curves) and 200-km (orange curves) SSMF propagation are reported, in order to highlight the different impact of the equalization for medium- to long-reach transmissions. In case of short SSMF links, a SNR improvement in the full modulation bandwidth is noticeable; after 200 km, on the other hand, the SNR increase is focused in the mid-frequency region, in particular in the 2-12 GHz range. The VE, therefore, acts where the fiber NLs have a greater impact on the SNR curve, i.e., close to the frequency dip. Actually, the VE behavior depends on the number of linear and non-linear taps and on the convergence parameters. It is possible to obtain an enhancement in the low-frequency region, but in this case the SNR improvement is strictly limited to a few GHz range and the overall increase in the achievable capacity is lower.

The change of the SNR curves impacts on the capacity performance through the bit loading procedure. To highlight the advantages related to the use of VE, FIGURE 12 shows the bit loading achievable in different system configurations. In particular, the performance is reported for both single and 25-GHz-spaced 7-channels transmissions for different propagation distances (BTB, 100 km, 200 km) with and without Volterra equalization. The complete description of the system configurations is reported in TABLE 3. The last column represents the number of bits transported by a single DMT symbol, obtained as the sum of the bits transported by all the signal subcarriers. Generally, the enhancement of the performance owing to VE exploitation appears as an increase of the number of transported bits per subcarrier in a wide frequency region. As expected by the SNR curve analysis previously reported, VE permits to increase the modulation order of subcarriers located in the low-medium frequency range. The performance enhancement is confirmed by the total number of transported bits by a DMT symbol: after 200-km SSMF propagation (configuration 10), the number of transported bits in case of VE use is still greater than the reference one achieved in BTB conditions without VE (configuration 1). In case of multi-channel propagation, a worsening of the achievable bit loading is noticed for all the system configurations with respect to the corresponding single-channel one. In particular, the reduction of the number of bits transported by the high-frequency subcarriers is caused by the presence of a residual linear crosstalk among the adjacent channels, owing to the very tight spacing of 25 GHz. However, the presence of VE leads to a general mitigation of the impact of SSMF propagation, permitting to obtain a limited reduction of the capacity even after 200 km (configuration 12) with respect to the reference condition (configuration 1).

Finally, FIGURE 13 reports an estimation of the SNR variation in function of the launch power in the 7-channel configuration. In particular, ΔSNR_{nonlin} (top row, FIGURE 13(a), 13(b)) represents the difference in the SNR values between linear and non-linear fiber propagation in case of absence of equalization, whereas ΔSNR_{eq} (bottom row, FIGURE 13(c), 13(d)) is calculated as the difference between the SNR profiles obtained with and without VE for the same launch powers, i.e., it represents the SNR variation caused by the equalizer. To obtain the ΔSNR achievable in case of VE corresponding to the respective reference linear propagation, it is required to sum up the ΔSNR_{nonlin} and the ΔSNR_{eq}. The ΔSNR variations are reported for two different SSMF

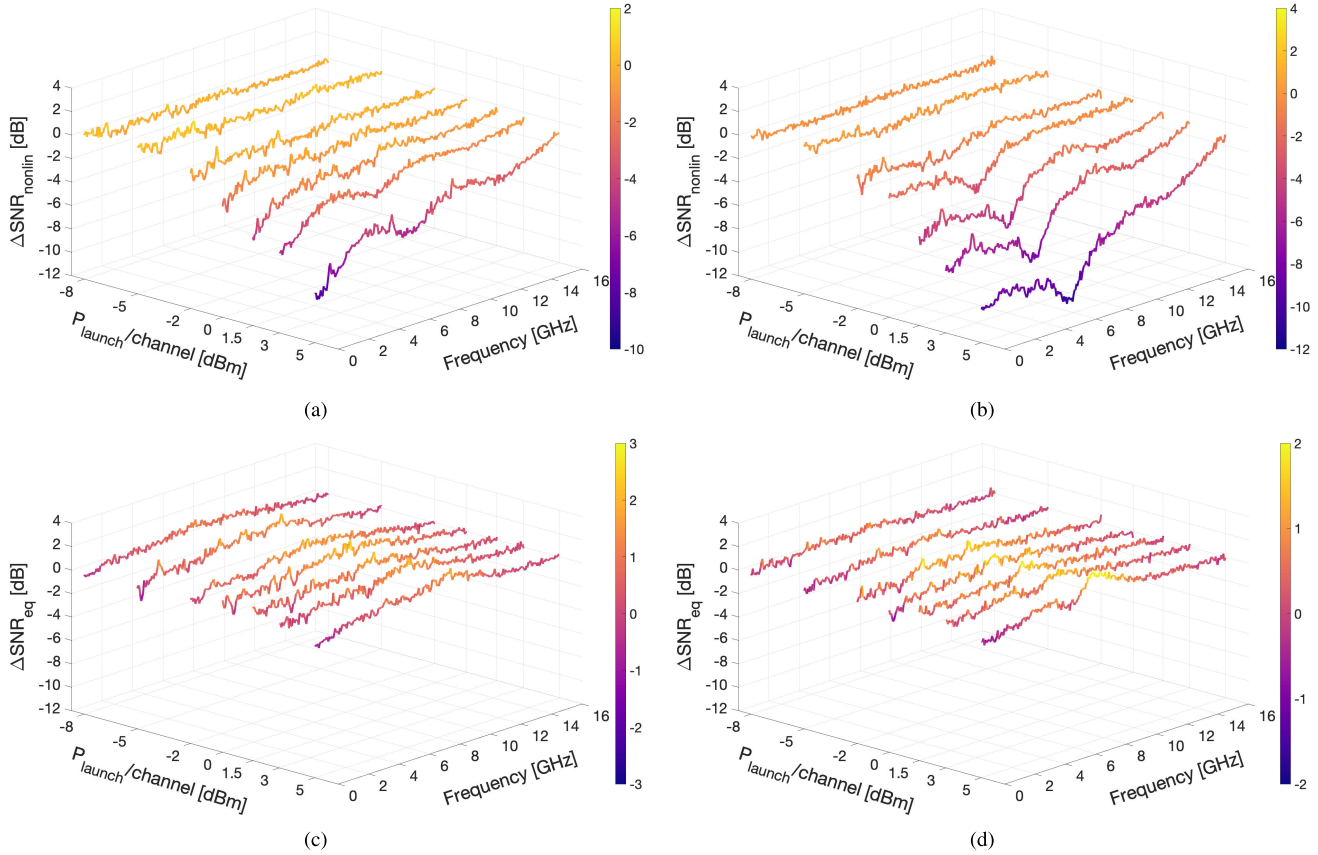

FIGURE 13. ΔSNR profiles obtained after 100 km (left column) and 200 km (right column) SSMF non-linear propagation without and with VE in case of 7 25-GHz-spaced channel transmission. The ΔSNR profiles in the top row ((a) and (b)) are defined as the difference of achievable SNRs in case of NL propagation without VE with respect to the multi-channel linear condition. In the bottom row ((c) and (d)), the difference between the SNRs achievable with and without the VE in case of NL propagation is reported.

lengths, 100 km (left column, FIGURE 13(a), 13(c)) and 200 km (right column, FIGURE 13(b), 13(d)). The impact of intra- and inter-channel fiber NLs is apparent in the top row: increasing the optical launch power, a clear distortion of the SNR profile appears both for 100-km and 200-km SSMF transmission. As expected, the SNR perturbation is stronger for the longest distance and NLs start to modify the ΔSNR_{nonlin} curve for lower launch powers. At low launch power the ΔSNR_{nonlin} is characterized by a flat behavior close to 0 dB, showing that in this power range the system performance depends only on the specific OSNR value. Increasing the optical power, the SNR NL-induced reduction is not uniform in the spectral domain. In particular, the low-frequency sub-carrier performance is impacted, leading to a decrease of the SNR value of 10 dB or more with respect to linear propagation in case of high launch powers. Moreover, as already pointed out, a second dip appears around 5-6 GHz. Therefore, the distortion of the SNR profile is far from a ''white noise'' like perturbation [38].

The effect of the VE on the DMT signal can be analyzed through FIGURE 13(b) and 13(d); in particular, in the mid frequency range the ΔSNR_{eq} shows an improvement of few dBs, revealing the spectral band of VE maximum gain. Still, due to the VE limited efficacy at low and high frequencies, the transmission performance cannot reach the linear propagation one. Moreover, for longer propagation distances the equalizer effectiveness progressively reduces even in the mid frequency range with an associated decrease of the transmission performance. At higher launch powers, the limited improvements in the mid-frequency region cannot counteract the SNR drop in the low-frequency range, thus the supported capacity decreases. However, as already mentioned, VE leads to an increase of the optimal launch power, thus an overall improvement of the capacity performance can be reached also thanks to a higher OSNR at the receiver.

V. CONCLUSION

The exploitation of DM VCSELs and COD can represent a solution for sustainable future high-capacity MANs. The use of multiple InP SC VCSELs covering the C-band with 25-GHz spacing allows to implement multi Tb/s DWDM transmitters with low cost, low power consumption and reduced footprint, whereas COD supports distances of hundreds of km, required for MAN applications. In this paper, VE effectiveness has been systematically studied to cope not

only with the distortions caused by the transmitter/receiver ends, but also to mitigate the impact of intra-channel nonlinear impairments allowing good performance also in presence of several tightly spaced DMT channels after propagation over hundreds of fiber kilometers. Experimental measures of 25-GHz-spaced WDM channels directly-modulated by a 20-GHz DMT signal over up to 200 km of SSMF have demonstrated the achievable performance with and without VE. The reported measurements have been used to validate a simulation tool, developed to provide a systematic analysis of the supported capacity per channel. The transmission of the proposed DMT-modulated VCSEL-based MAN has been simulated in single-channel and multi-channel (up to 7 co-propagating channels) conditions up to 200-km SSMF transmission, with and without VE. In case of single-channel propagation, intra-channel nonlinear impairments are compensated by VE enabling the use of higher launch powers, improving the OSNR at the receiver and, hence, increasing the supported capacities. Up to 11% improvement of the capacity per VCSEL is possible including the compensation of distortions introduced by signal generation and detection and of SPM impairments. When dense 25-GHz WDM transmission is considered, despite inter-channel NL accumulation, VE employment actually allows an overall capacity increase of 13% after 200 km with respect to VE absence. The obtained results prove the effectiveness of the VE for extended reaches assuring 50 Gb/s rate per polarization per VCSEL, as targeted for the considered sustainable multi-Tb/s MAN.

ACKNOWLEDGMENT

The authors would like to thank Micram for the sponsorship and Tektronix for the OM4245 equipment.

REFERENCES

[1] N. Kikuchi, R. Hirai, and T. Fukui, "Non-linearity compensation of high-speed PAM4 signals from directly-modulated laser at high extinction ratio," in *Proc. 42nd Eur. Conf. Opt. Commun.*, Sep. 2016, pp. 1–3.

[2] N.-P. Diamantopoulos, W. Kobayashi, H. Nishi, K. Takeda, T. Kakitsuka, and S. Matsuo, "56-Gb/s VSB-PAM-4 over 80-km using 1550-nm EA-DFB laser and reduced-complexity nonlinear equalization," in *Proc. Eur. Conf. Opt. Commun. (ECOC)*, Sep. 2017, pp. 1–3.

[3] V. Volterra, *Theory of Functionals and of Integral and Integro-differential Equations*. New York, NY, USA: Dover, 1959.

[4] F. P. Guiomar, S. B. Amado, C. S. Martins, and A. N. Pinto, "Time-domain Volterra-based digital backpropagation for coherent optical systems," *J. Lightw. Technol.*, vol. 33, no. 15, pp. 3170–3181, Aug. 1, 2015.

[5] N.-P. Diamantopoulos, H. Nishi, W. Kobayashi, K. Takeda, T. Kakitsuka, and S. Matsuo, "On the complexity reduction of the second-order Volterra nonlinear equalizer for IM/DD systems," *J. Lightw. Technol.*, vol. 37, no. 4, pp. 1214–1224, Feb. 15, 2019.

[6] W.-J. Huang, W.-F. Chang, C.-C. Wei, J.-J. Liu, Y.-C. Chen, K.-L. Chi, C.-L. Wang, J.-W. Shi, and J. Chen, "93% complexity reduction of Volterra nonlinear equalizer by ℓ_1-regularization for 112-Gbps PAM-4 850-nm VCSEL optical interconnect," in *Proc. Opt. Fiber Commun. Conf. Expo. (OFC)*, Mar. 2018, pp. 1–3.

[7] F. P. Guiomar, S. B. Amado, N. J. Muga, J. D. Reis, A. L. Teixeira, and A. N. Pinto, "Simplified Volterra series nonlinear equalizer by intra-channel cross-phase modulation oriented pruning," in *Proc. 39th Eur. Conf. Exhib. Opt. Commun. (ECOC)*, Sep. 2013, pp. 1–3.

[8] L. Zhang, X. Hong, X. Pang, O. Ozolins, A. Udalcovs, R. Schatz, C. Guo, J. Zhang, F. Nordwall, K. M. Engenhardt, U. Westergren, S. Popov, G. Jacobsen, S. Xiao, W. Hu, and J. Chen, "Nonlinearity-aware 200 Gbit/s DMT transmission for C-band short-reach optical interconnects with a single packaged electro-absorption modulated laser," *Opt. Lett.*, vol. 43, no. 2, p. 182, Jan. 2018.

[9] C. Bluemm, M. Schaedler, M. Kuschnerov, F. Pittala, and C. Xie, "Single carrier vs. OFDM for coherent 600 Gb/s data centre interconnects with nonlinear equalization," in *Proc. Opt. Fiber Commun. Conf. Exhib. (OFC)*, Mar. 2019, pp. 1–3.

[10] N.-P. Diamantopoulos, H. Yamazaki, S. Yamaoka, M. Nagatani, H. Nishi, H. Tanobe, R. Nakao, T. Fujii, K. Takeda, T. Kakitsuka, H. Wakita, M. Ida, H. Nosaka, F. Koyama, Y. Miyamoto, and S. Matsuo, "Net 321.24-Gb/s IMDD transmission based on a >100-GHz bandwidth directly-modulated laser," in *Proc. Opt. Fiber Commun. Conf. Exhib. (OFC)*, Mar. 2020, pp. 1–3.

[11] J. Jignesh, T. A. Eriksson, M. Chagnon, B. Corcoran, A. J. Lowery, F. Buchali, and H. Bülow, "Transmitter-side Volterra filtering for increased dispersion tolerance in 56 gbaud PAM-4 systems," in *Proc. Opt. Fiber Commun. Conf. Expo. (OFC)*, Mar. 2018, pp. 1–3.

[12] P. Boffi, P. Parolari, A. Gatto, M. Rapisarda, M. S. Moreolo, L. Nadal, J. M. Fabrega, N. Calabretta, R. Stabile, N. Tessema, D. Larrabeiti, J. P. Fernández-Palacios, G. Otero, C. Neumeyr, G. Delrosso, S. Bhat, K. Solis-Trapala, and G. Parladori, "Multi-Tb/s sustainable MAN scenario enabled by VCSEL-based innovative technological solutions," *Proc. SPIE*, vol. 11308, pp. 86–93, Jan. 2020.

[13] M. Svaluto Moreolo et al., "SDN-enabled sliceable BVT based on multicarrier technology for multiflow rate/distance and grid adaptation," *J. Lightw. Technol.*, vol. 34, no. 6, pp. 1516–1522, Mar. 15, 2016.

[14] L. Zhang et al., "Nonlinearity tolerant high-speed DMT transmission with 1.5-μm single-mode VCSEL and multi-core fibers for optical interconnects," *J. Lightw. Technol.*, vol. 37, no. 2, pp. 380–388, Jan. 15, 2019.

[15] F. Barrami, Y. Le Guennec, E. Novakov, and P. Busson, "Impact of VCSEL nonlinearity on discrete MultiTone modulation: Quasi-static approach," in *Proc. 21st Int. Conf. Telecommun. (ICT)*, May 2014, pp. 113–118.

[16] T. Aalto, M. Cherchi, M. Harjanne, S. Bhat, P. Heimala, F. Sun, M. Kapulainen, T. Hassinen, and T. Vehmas, "Open-access 3-μm SOI waveguide platform for dense photonic integrated circuits," *IEEE J. Sel. Topics Quantum Electron.*, vol. 25, no. 5, pp. 1–9, Sep. 2019.

[17] G. Delrosso and S. Bhat, "Development and scalability of a 2 Tb/s data transmission module based on a 3μm SOI silicon photonics platform," in *Proc. 22nd Int. Conf. Transparent Opt. Netw. (ICTON)*, vol. 25, Jul. 2020, pp. 1–5.

[18] P. Parolari, A. Gatto, M. Rapisarda, F. Lipparini, C. Neumeyr, M. S. Moreolo, and P. Boffi, "Transmitter and receiver solutions for VCSEL exploitation in access and metro networks," *Proc. SPIE*, vol. 11712, pp. 20–26, Mar. 2021.

[19] A. Gatto, M. Rapisarda, P. Parolari, M. Svaluto Moreolo, C. Neumeyr, and P. Boffi, "Long-wavelength VCSEL-based system exploiting direct DMT modulation and coherent detection for multi-Tb/s metro link," in *Proc. 24th Int. Conf. Opt. Netw. Design Modeling (ONDM)*, 2020, pp. 1–3.

[20] P. Parolari, A. Gatto, M. Rapisarda, F. Lipparini, C. Neumeyr, M. S. Moreolo, and P. Boffi, "Preliminary assessment of photonic solutions based on C-band VCSELs for multi-Tb/s metro networks," in *Proc. 22nd Int. Conf. Transparent Opt. Netw. (ICTON)*, Jul. 2020, pp. 1–5.

[21] M. S. Moreolo, J. M. Fabrega, L. Nadal, R. Martinez, R. Casellas, J. Vilchez, R. Munoz, R. Vilalta, A. Gatto, P. Parolari, P. Boffi, C. Neumeyr, D. Larrabeiti, G. Otero, and J. P. Fernandez-Palacios, "Programmable VCSEL-based photonic system architecture for future agile Tb/s metro networks," *J. Opt. Commun. Netw.*, vol. 13, no. 2, pp. A187–A199, Feb. 2021.

[22] P. Parolari, A. Gatto, C. Neumeyr, and P. Boffi, "Flexible transmitters based on directly modulated VCSELs for next-generation 50G passive optical networks," *J. Opt. Commun. Netw.*, vol. 12, no. 10, pp. D78–D85, 2020.

[23] M. S. Moreolo, L. Nadal, J. M. Fabrega, F. J. Vilchez, C. Neumeyr, A. Gatto, P. Parolari, and P. Boffi, "VCSEL-based sliceable bandwidth/bitrate variable transceivers," *Proc. SPIE*, vol. 10946, pp. 26–32, Feb. 2019.

[24] J. G. Proakis and M. Salehi, *Digital Communications*, vol. 4. New York, NY, USA: McGraw-Hill, 2001.

[25] M. Müller, W. Hofmann, T. Grundl, M. Horn, P. Wolf, R. D. Nagel, E. Ronneberg, G. Bohm, D. Bimberg, and M.-C. Amann, "1550-nm high-speed short-cavity VCSELs," *IEEE J. Sel. Topics Quantum Electron.*, vol. 17, no. 5, pp. 1158–1166, Sep. 2011.
[26] C. Xie, S. Spiga, P. Dong, P. Winzer, M. Bergmann, B. Kögel, C. Neumeyr, and M.-C. Amann, "400-Gb/s PDM-4PAM WDM system using a monolithic 2×4 VCSEL array and coherent detection," *J. Lightw. Technol.*, vol. 33, no. 3, pp. 670–677, Feb. 1, 2015.
[27] M. Rapisarda, A. Gatto, P. Martelli, P. Parolari, C. Neumeyr, M. S. Moreolo, J. M. Fabrega, L. Nadal, and P. Boffi, "Impact of chirp in high-capacity optical metro networks employing directly-modulated VCSELs," *Photonics*, vol. 5, no. 4, p. 51, Nov. 2018.
[28] C. Pulikkaseril, L. A. Stewart, M. A. F. Roelens, G. W. Baxter, S. Poole, and S. Frisken, "Spectral modeling of channel band shapes in wavelength selective switches," *Opt. Exp.*, vol. 19, no. 9, pp. 8458–8470, Apr. 2011.
[29] P. S. Chow, J. M. Cioffi, and J. A. C. Bingham, "A practical discrete multitone transceiver loading algorithm for data transmission over spectrally shaped channels," *IEEE Trans. Commun.*, vol. 43, nos. 2–4, pp. 773–775, Feb. 1995.
[30] M. S. Moreolo et al., "SDN-enabled sliceable BVT based on multicarrier technology for multi-flow rate/distance and grid adaptation," in *Proc. Eur. Conf. Opt. Commun. (ECOC)*, Sep. 2015, pp. 1–3.
[31] A. Gatto, M. Rapisarda, P. Parolari, and P. Boffi, "Discrete multitone modulation for short-reach mode division multiplexing transmission," *J. Lightw. Technol.*, vol. 37, no. 20, pp. 5185–5192, Oct. 15, 2019.
[32] A. Gatto, A. Boletti, P. Boffi, and M. Martinelli, "Adjustable-chirp VCSEL-to-VCSEL injection locking for 10-Gb/s transmission at 1.55 μm," *Opt. Exp.*, vol. 17, no. 24, pp. 21748–21753, 2009.
[33] R. Rodes, M. Mueller, B. Li, J. Estaran, J. B. Jensen, T. Gruendl, M. Ortsiefer, C. Neumeyr, J. Rosskopf, K. J. Larsen, M.-C. Amann, and I. T. Monroy, "High-speed 1550 nm VCSEL data transmission link employing 25 GBd 4-PAM modulation and hard decision forward error correction," *J. Lightw. Technol.*, vol. 31, no. 4, pp. 689–695, Feb. 15, 2013.
[34] S. Spiga, W. Soenen, A. Andrejew, D. M. Schoke, X. Yin, J. Bauwelinck, G. Boehm, and M.-C. Amann, "Single-mode high-speed 1.5-μm VCSELs," *J. Lightw. Technol.*, vol. 35, no. 4, pp. 727–733, Feb. 15, 2017.
[35] T. L. Koch and J. E. Bowers, "Nature of wavelength chirping in directly modulated semiconductor lasers," *Electron. Lett.*, vol. 20, nos. 25–26, pp. 1038–1040, Dec. 1984.
[36] S. van der Heide, A. Albores-Mejia, F. Gomez-Agis, B. Docter, and C. Okonkwo, "112-Gbit/s single side-band PAM-4 transmission over inter-DCI distances without DCF enabled by low-complexity DSP," in *Proc. Eur. Conf. Opt. Commun. (ECOC)*, Sep. 2017, pp. 1–3.
[37] T.-K. Chiang, N. Kagi, M. E. Marhic, and L. G. Kazovsky, "Cross-phase modulation in fiber links with multiple optical amplifiers and dispersion compensators," *J. Lightw. Technol.*, vol. 14, no. 3, pp. 249–260, Mar. 1996.
[38] R. Dar, M. Feder, A. Mecozzi, and M. Shtaif, "Properties of nonlinear noise in long, dispersion-uncompensated fiber links," *Opt. Exp.*, vol. 21, no. 22, pp. 25685–25699, Nov. 2013.

ALBERTO GATTO (Member, IEEE) received the M.S. degree in telecommunication engineering and the Ph.D. degree in information technology from the Politecnico di Milano, in 2007 and 2011, respectively.

From May 2013 to November 2014, he was a member of the Virgo Team, Laboratoire APC "Astroparticule et Cosmologie," Universite Paris Diderot, actively involved in the first observation of gravitational waves. He is currently an Assistant Professor with the Department of Electronics, Information, and Bioengineering, Politecnico di Milano, where he is also with the Optical Communication Laboratory, PoliCom. His current research interests include quantum key distribution integration in classical communication systems, short-reach and metro optical communications based on advanced modulation formats and low cost/low complexity solutions, and very high-capacity space-division multiplexing optical systems exploiting multi-core and few-mode fibers. He is the author of more than 150 papers in the area of optical communication systems and networks, published in international journals and conference proceedings.

Dr. Gatto serves as a TPC member and/or a reviewer for several IEEE/OSA conferences and IEEE/OSA and Elsevier journals.

ANTONINO FAVANO received the M.Sc. degree (cum laude) in telecommunication engineering and the Ph.D. degree in information technology from the Politecnico di Milano, Milan, Italy, in 2018 and 2023, respectively.

He is currently a Research Fellow with the Politecnico di Milano, working in the field of error-correcting codes for emerging memories. His main research interests include coding theory, information theory, and the broad area of wireless and optical communications.

PAOLA PAROLARI (Senior Member, IEEE) received the M.S. degree (cum laude) in telecommunication engineering and the Ph.D. degree in information engineering from the Politecnico di Milano, in 1997 and 2001, respectively.

She is currently an Associate Professor with the Dipartimento Elettronica Informazione e Bioingegneria, Politecnico di Milano, where she is also with the Optical Communication Laboratory, PoliCom. She is also a Co-Founder of the start-up company Cohaerentia. From 2011 to 2014, she has been the WP Leader of the FP7 EU Project ERMES. From 2017 to 2021, she has been the Project Manager of the H2020 EU Project PASSION. She is now involved in the EU Digital Europe Project QUID and in the PRIN Projects FIRST and SURENET. Her research interests include optical amplifiers, all-optical processing, highly spectrally efficient transmission systems, advanced modulation formats, access network technologies as WDM and OFDM PON, new architectures for the mobile Fronthaul, partial MIMO-based mode division multiplexing, and coexistence of classical and QKD systems. She has co-authored more than 160 papers in international journals and conferences and she holds 13 international patents.

Dr. Parolari has been/is a member of the Technical Program Committee of leading international conferences in the field of optical communications, such as OFC, ECOC, ONDM, PSC, and CLEO-PR. Since 2019, she has been a Publicity Editor of the IEEE/OSA JOURNAL OF LIGHTWAVE TECHNOLOGY.

CHRISTIAN NEUMEYR, photograph and biography not available at the time of publication.

MARCO FERRARI (Member, IEEE) was born in Milan, Italy, in 1971. He received the Laurea degree (M.S. equivalent) (cum laude) in telecommunications engineering and the Ph.D. degree in electronics and communication engineering from the Politecnico di Milano, Italy, in 1996 and 2000, respectively.

Since 2001, he has been a Researcher with the Istituto di Elettronica e di Ingegneria dell'Informazione e delle Teelcomunicazioni (IEIIT), Consiglio Nazionale delle Ricerche (CNR), Politecnico di Milano. In 2002, he was an EPRSC Research Fellow with the University of Plymouth, U.K. He has co-authored approximately 70 scientific publications on leading international journals and conference proceedings and few patents. His main research interests are in channel coding, information theory, and digital transmission.

LUCA BARLETTA (Member, IEEE) received the M.S. degree (cum laude) in telecommunications engineering and the Ph.D. degree in information engineering from the Politecnico di Milano, Milan, Italy, in 2007 and 2011, respectively.

In 2012, he was a Visiting Researcher with the Bell Laboratories, Alcatel-Lucent, Holmdel, NJ, USA, working on long-haul fiber-optic communications. From 2012 to 2015, he was a Postdoctoral Researcher with the Institute for Advanced Study and the Institute for Communications Engineering, Technische Universitaet Muenchen, Munich, Germany, working on capacity for continuous-time phase-noise channels. Since 2019, he has been with the Politecnico di Milano, where he is currently an Associate Professor, working in the broad field of information and communication theory.

Dr. Barletta received the IEEE Communications Society Charles Kao Award for the paper Machine-Learning Method for Quality of Transmission Prediction of Unestablished Lightpaths', appeared on the IEEE/OSA JOURNAL OF OPTICAL COMMUNICATIONS AND NETWORKING, Vol. 10, No. 2, in 2020.

MAURIZIO MAGARINI (Member, IEEE) received the M.Sc. and Ph.D. degrees in electronic engineering from the Politecnico di Milano, Milan, Italy, in 1994 and 1999, respectively.

In 1994, he was granted the TELECOM Italia Scholarship Award for his M.Sc. Thesis. He was a Research Associate with the Dipartimento di Elettronica, Informazione e Bioingegneria, Politecnico di Milano, from 1999 to 2001, where he was an Assistant Professor, from 2001 to 2018. Since June 2018, he has been an Associate Professor with the Politecnico di Milano. From August 2008 to January 2009, he spent a sabbatical leave with the Bell Laboratories, Alcatel-Lucent, Holmdel, NJ, USA. His research interests include communication and information theory, synchronization, channel estimation, equalization and coding applied to wireless and optical communication systems, molecular communications, massive MIMO, study of waveforms for 5G cellular systems, vehicular communications, wireless sensor networks for mission critical applications, and wireless networks using unmanned aerial vehicles and high-altitude platforms. He has authored or co-authored more than 120 journals and conference papers. He was a co-recipient of two best paper awards. He is an Associate Editor of IEEE ACCESS, *IET Electronics Letters*, and *Nano Communication Networks* (Elsevier). He has been involved in several European and national research projects.

PIERPAOLO BOFFI (Senior Member, IEEE) is currently an Associate Professor with the Dipartimento di Elettronica, Informazione e Bioingegneria, Politecnico di Milano, Milan, Italy, where he is the responsible of the Optical Communications Laboratory, PoliCom (www.policom.deib.polimi.it). He is also the Co-Founder of Cohaerentia, a spin-off company of the Politecnico di Milano. In 1997, he was a Visiting Researcher with Caltech, Pasadena, CA, USA. His expertise is on optical fiber communications and his main research activities include very high capacity optical systems for applications both in the long-haul transport network and in the metro-regional and access network. On these topics, he has published more than 250 peer-reviewed papers in international journals and conference proceedings. He is the inventor of 17 international patents filed in the field of optical communication systems. He leads several industrial projects and was involved in the scientific and technical activities of several national and European research projects. He was the Coordinator of the H2020 Project PASSION (www.passion-project.eu).

Open Access funding provided by 'Politecnico di Milano' within the CRUI CARE Agreement